Analysis of Turbulent Concentration Fields in a Stirred Chemical Reactors Using a RNG Turbulence Model and Optical Tomography

J. N. Al-Saeedi, Tiyun Xu and R. W. Pike*

Department of Chemical Engineering, Louisiana State University, Baton Rouge, LA 70803

ABSTRACT

A new method of measuring turbulent concentration fields in a stirred chemical reactor was developed using image processing and tomography. The system used the color change reaction of HCl and NaOH with phenol phthalein indicator to measure the concentration field at 27.9 million points at 1/30th sec. intervals in a stirred chemical reactor noninvasively using images from two perpendicular CCD video cameras. The reactor had a standard configuration (29.21 cm. dia., Rushton turbine). The tomographic algorithm, algebraic reconstruction technique (ART), was used to reconstruct the three-dimensional concentration distribution from digitized video images (329x329 pixels) of side views of the reactor. A plume of color was generated by injecting 5 ml of 1.0 N NaOH at the tip of the impeller an acidic solution in the reactor, and this plume moves around the reactor and collapses as the base is neutralized in 2.5 sec. at an impeller speed of 200 rpm. The concentration fields were reconstructed in 1/30th sec. intervals, and results are presented in several different forms, e.g. concentration at key points as a function of time. Validation included reconstruction of a stationary object, recalculation of projections and minimizing the error variance.

The three-dimensional turbulent velocity and concentration distributions were simulated in a stirred reactor. The sliding mesh technique, finite volume method and RNG k-ε model were used to perform the simulation. Also, a grid evaluation was performed and simulation results were not affected by the grid number of simulation system. For the simulation of turbulent flow, the RNG k-ε model proved to be one of the accurate models to simulate fluid flow. The velocity simulation results were close to the experimental data of previous researchers. The RNG k-ε model can be used with confidence to simulate the fluid flow in most situations. For the simulation of the turbulent chemical reaction in a stirred tank, the simulation concentration trend matches the concentration field for the chemical reaction experiments.

KEYWORDS

- Tomography.
- Stirred tanks.
- Concentration distributions.
- Turbulent flow.
- Mixing.

---

*Author to whom correspondence should be addressed. Submitted for publication

Introduction

Turbulent mixing in a stirred reactor is an important operation in chemical processing and has been widely used to perform many functions that involve simultaneous momentum, heat, and mass transfer, such as absorption, extraction, dissolution, multi-phase chemical reactions, including polymerization and fermentation (Paul,Atiemo-Obeng and Kresta, 2004). The fluid dynamics for turbulent flow of a liquid in a tank stirred with a Rushton turbine is reasonably well understood. Research continues to understand instabilities in stirred vessels using laser anemometry and flow visualization (Galletti, Paglianti, Lee and Yianneskis, 2004) and effect of mixing on product distribution in batch stirred reactors using laser velocimetry and CFD (Akiti and Armenante, 2004), for example. However, field measurements are needed for the turbulent concentration distributions that be used to evaluate closure models for the time-averaged terms of the fluctuating components in the time-averaged species continuity equation. Optical tomography and image processing offer a non-invasive technique that enables the measurement of three-dimensional concentration fields spatially and temporally in a stirred chemical reactor from a set of two-dimensional projections. With these measurements, accuracy of models used in the solution of the turbulent, time-averaged species continuity equation can be evaluated.

In optical tomography rays from a radiation source pass through the medium along straight lines in the fluid in the reactor and are measured at the projection view or image plane as illustrated in Figure 1. The intensity of the ray is diminished according to the Bouguer-Lambert-Beer law as evaluated by a line integral along the ray (Hesselink, 1989). The measurement volume is radiated with a suitable source, and the intensity of the radiation is measured at the plane across from the source. The measurements at the plane across from the source are referred to as projections as shown in Figures 1 and 2. Optical tomography requires a transparent fluid, and the variations in the fluid optical properties are caused by either velocity, temperature or concentration fields. In this work concentration fields were measured using a color change reaction in a stirred chemical reactor shown in Figure 3, and a description is given of the tomographic methods developed for a stirred reactor to reconstruct the turbulent concentration fields. These results were used to study the concentration fluctuations at various points in the reactor and evaluate turbulent terms in the species continuity equation using the CFD code Fluent.

Reviews of applications of tomography to stirred vessels have been given by Galletti, Paglianti, Lee and Yianneskis, (2004), Mavros, (2001) and Herman, et al., (1992). Field measurements use tomography and holography to measure the concentration distribution simultaneously. Tomography is superior to point measurements that involve moving a probe around in the flow. The methods include optical, x-ray tomography, electrical resistance and ultrasonic tomography. Verschuren, et al., (2002) used planar laser-induced fluorescence to measure the mean concentration and concentration variance of a tracer dye excited by a laser sheet in a Rushton turbine stirred vessel and compared their result with a turbulent mixer model. Holden, et al., (1998) described electrical resistance tomography measurements in a plant-scale stirred vessel using the dispersion of a brine pulse tracer to monitor the mixing processes. Reconstruction of the concentration field used the linear back-projection method. Buchmann and Mewes., (1998) reconstructed the concentration and local intensity of segregation at 36,600 elements of an inert and reacting dye in a Rushton turbine stirred vessel using three CCD cameras and the ART algorithm. Three studies reporting field measurements in stirred vessels

using tomography were William, et al., (1987) who applied electrical impedance tomography (EIT) to measure concentration profiles of a saline solution in four planes in a 30 dm^3 tank with standard Rushton turbine and four equi-spaced baffles. Haarde (1989) used laser tomography to measure the concentration field of a turbulent jet of dye injected into a quiscent liquid in a circular vessel with two synchronized cameras where the film was digitized and scanned to give projections for reconstructing the concentration field. Ostendorf and Mews (1988) measured the temperature distribution in laminar and turbulent flow in a vessel stirred with a Rushton turbine using high and medium viscosity solutions where a small volume of heated liquid was added to the vessel, and temperature isotherms were measured using the apparatus described by Haarde (1989).

Turbulent Flow and Chemical Reactions in Stirred Reactors

There have been numerous studies on turbulent flow in stirred reactors, and the Handbook of Fluid Mixing (Paul,Atiemo-Obeng and Kresta, 2004) includes reviews on turbulence in mixing applications, computational fluid mixing, gas-liquid mixing in turbulent systems, and mixing with chemical reactions. The book by Fox (2003) on computational models for turbulent reacting flows devotes a chapter to closures for the chemical source term emphasizing probability density functions (PFD). A detailed review by Ranade (1995) described turbulent mixing affects chemical reactions. The computational fluid dynamics code Fluent (1995) has options for the k-ε, Reynolds stress and renormalization group (RNG) k-ε models and uses the model developed by Magnussen and Hjertager (1976) for closure of the chemical source term.

The effect of turbulence depends on type and rate of reaction and how the reactants injected into the reactor, among others. When a chemical reaction takes place under turbulent flow conditions, turbulent motion brings reactants together and disperses products. Chemical reactions cannot take place between species unless they are mixed, and the traditional chemical reaction kinetic models for turbulent flow are based on the concepts of macro and micromixing (Tatterson 1990). Usually, these turbulent reaction models usually involve several unknown parameters that are fitted using experimental data.

Measurements of the concentration fluctuations in a stirred chemical reactor can be used to understand the interactions of the turbulence and the kinetics of a reaction. The time-smoothed species continuity equation for turbulent flow of an isothermal, binary-fluid mixture with constant density, diffusivity, and viscosity given by Bird, Stewart and Lightfoot, 2002 is:

$$-\frac{dC_A}{dt} = (\nabla \cdot \bar{J}_A^{(1)}) + (\nabla \cdot \bar{J}_A^{(t)}) - r_A \qquad (1)$$

The terms on the right hand side of the equation represent the gradient of the time averaged laminar and turbulent fluxes and the time-averaged chemical reaction rate. Studies that have been preformed to develop a description of the turbulent mass flux terms include Vassilatos and Toor (1965), Toor (1969), Mao and Toor (1970), Toor (1975), Patterson (1981) and Ranade and Bourne (1991).

For the second order reaction, A+B→ products, the chemical reaction rate expression can be written as:

$$r_A = k C_A C_B \quad (2)$$

By using Reynolds rules of averaging, Equation (2) becomes:

$$\overline{r_A} = k(\overline{C}_A\overline{C}_B + \overline{c_A c_B}) \quad (3)$$

In this equation, $\overline{C}_A$ and $\overline{C}_B$ are the time-averaged values of the species concentration C_A and C_B.

The term $\overline{c_A c_B}$ represent the product of co-variances of concentrations from their time-averaged values. Usually, this term depends upon both the turbulent mixing and the chemical reaction, and it represents a measure of the concentration fluctuations in the mixing process.

Equation for the Turbulent Chemical Reaction in a Stirred Tank

The term $\overline{c_A c_B}$ usually depends upon both the turbulent mixing and the chemical reaction. $\overline{c_A c_B}$ can be positive or negative depending on whether the reactants are premixed or not (Toor, 1975). When the species are perfectly mixed, $\overline{c_A c_B}$ will approach zero. Otherwise, if the species are not perfectly mixed, this term will be negative and reduce the reaction rate. Therefore, the time average reaction rate will be greater if the reactants are premixed, less if they are not (Toor, 1975).

Very rapid, rapid and slow reactions that present different problems. These correspond to reaction rates much faster than the rate of mixing, reaction rates of the same order as the rate of mixing, and reaction rates much slower than the rate of mixing. The third case is the simplest, because a slow reaction is one in which $\overline{c_A c_B} << \overline{C}_A\overline{C}_B$. For very slow reaction $\overline{c_A c_B}$ does not affect the chemical reaction rate, and the term $\overline{c_A c_B}$ can be neglected.

Several closure methods have been described. Toor, 1975 proposed a closure model for a very rapid reaction that does not include the radial gradients of time-averaged quantities. Ranade and Bourne (1991) proposed another closure approximation for a slow reaction where $\overline{c_A c_B} = \sqrt{c_A^2\, c_B^2}$ which is based on statistical theory. Both Toor (1969) and Ranade and Bourne (1991) reported good agreement between model predictions and experimental data collected in a plug flow reactor and an agitated tank, respectively. Patterson(1981) proposed the another model based on statistical theory that had $\overline{c_A c_B} = \overline{c_A^2}\ (1 - \gamma)/[\beta\ (1 + \gamma)$ where $\beta = -C_{A0}/C_{B0}$ and $\gamma = -(\beta\ \overline{C}_A\overline{C}_B - \overline{c_A^2}\ )/(\beta\ \overline{C}_A\overline{C}_B + \overline{c_A^2}\ )$.

Bakker and Fasano (1994) reported simulated turbulent mixing and chemical reaction in stirred tanks with a CFD code. The mixing and transport of chemical species were calculated

from the following species continuity equation and Equation 4 gives the closure model they used.

$$R_{ki} = kM_i \prod_j \frac{\rho X_j}{M_j} \tag{4}$$

The reaction rate used in the species continuity equation was the minimum of the kinetic reaction rate R_{ki} and the turbulent mixing rate R_{mi}. In regions with high turbulent levels, the reaction rate is not limited by small scale mixing. In regions with low turbulent levels, small scale mixing may be slow and limit the reaction rate. The reaction rate is selected by the following equation.

$$R_{mi} = (M_i A_{mn} \frac{\varepsilon}{k}) \cdot \text{minimum} \qquad (\frac{\rho X_j}{\nu_j M_j})_{reac\,tan\,ts}) \tag{5}$$

Here X_i is the mass fraction of chemical species i, M_i is the molecular weight of species i and A_{mn}
is an empirically determined model constant for reaction n. In the reaction system, ν is +1 for products, and k is the kinetic rate constant of the reaction.

Ziman and Middleton (1990) developed the following equation based on micromixing concepts for the mean reaction rate of a simple step, second order reaction in an agitated tank where τ_m is the micromixing time..

$$\overline{R_A} = \frac{1}{\tau_m} \min \quad (C_A, C_B) \tag{6}$$

$$\tau_m = \frac{Sc}{2Sc + 1} [4 \frac{k}{\varepsilon} + 3.08(\frac{\mu}{\rho\varepsilon})^{\frac{1}{2}} \ln Sc] \tag{7}$$

This closure model was used in a k-ε turbulent model. Their predictions were for conversion in a stirred reactor, in which micromixing and macromixing control the reaction. Conversion depends on the stirred speed and is affected by macromixing. Predicted and experiment data of conversion were within the range of 50%.

The Fluent CFD code includes the turbulent micromixing model R_{im} given by Equation 8 proposed by Magnussen and Hjertager (1976).

$$R_{im} = C\rho \frac{\varepsilon}{k} \sum_i \frac{M_i}{\nu_{ik}} \tag{8}$$

Here C is an empirical constant (2.0 for products and 4.0 for reactants). The Fluent code selects the smaller of the two from this model and the kinetics of the reaction

In conclusion, methods was to model and verify the accuracy of the term $\overline{c_A c_B}$ have used simple geometry such as tubular reactor and one or two dimensional flow by comparing

simulation results to experiment data . Also, the minimum of the kinetic reaction rate R_{Ki} and turbulent mixing rate R_{mi} has been used for premixed and diffusion problems. In his work, Equations 6 and 7 will be used for the micromixing rate because it was used successfully for three-dimensional simulation of turbulent flow in baffled stirred reactors by Ziman and Middleton (1990).

RNG Turbulent Flow Model

The k-ε model based on Renormalization-Group (RNG) theory developed by Yolhot and Orszg(1986) differs from the k-ε two equation turbulent model in that constants and functions in the RNG model are evaluated by theory. RNG theory can solve the low Reynolds number (e.g. near wall) flow without the use of wall functions. Also, it provides improved predictions of near wall flows, flows with high streamline curvature and high strain rate, wall heat/mass transfer, wake flow and vortex shedding behavior, Fluent (1995).

Boundary Conditions and Sliding Mesh Method

The sliding mesh method has been applied to the simulation of fluid flow in a stirred tank by Perng and Murthy (1992), Demicdzic and Peric (1990), Chin (1992), Armenante and Chou (1996) and Harvey and Rogers (1996). These studies showed that simulation results compared to the experimental results using laser Doppler velocimetry (LDV) gave very good agreement with experimental data for velocity profiles in baffled vessels with single and double pitched-blade turbines. The advantage of the moving mesh method is that a single mesh is used for both stationary and moving parts and provides a means to solve the exact moving boundary conditions. Those parts of the mesh attached to the impeller move with the impeller and cause the mesh to deform as shown in Figure 4. When mesh deformation becomes acute, the grid is regenerated in accordance with the space conservation law. The moving grid technique, sliding mesh method. The jet model for the impeller stream is no longer required with a sliding mesh. The sliding mesh capability in the Fluent CFD code was used in this work.

For a three-dimensional flow field in an agitated vessel, the boundary conditions are needed for the solutions to governing equations. For the agitated vessel with a centrally located impeller, the boundary conditions are shown on a diagram for the flow in the vessel in Figure 5. When investigating velocity distributions in a stirred vessel, due to symmetry, a quarter or half of an agitated vessel is selected as the calculation domain. For the study of chemical reaction in a stirred tank with a point injection for chemical reactants, the entire geometry is used in the simulation, since the concentration distribution will not be symmetrical.

Referring to Figure 5, the shear stress between the air and liquid at the top of the liquid is sufficiently small to have the velocity gradients, with respect to z, be zero. Also, the other z-gradients, i.e., k and ε are taken as zero. In addition, the axial velocity is zero since there is no flow across the interface. The species concentration gradients, with respect to z, are zero, since there is no mass flux across the interface. Species concentration gradients, with respect to r, are zero at the tank wall; with respect to z, at the tank bottom; with respect to θ, at the baffles because of no flux across these solid surfaces. At the faces of stationary solids, such as the tank wall, tank bottom, and baffles, the no slip conditions apply, and the three velocity components are equal to zero there. Velocity fluctuations must vanish at stationary rigid surfaces, and both k

and ε are equal to zero there.

These boundary conditions also apply for the interior of the rotating solids, such as the shaft of the impeller. At the surface of the shaft, the axial and radial velocities are zero, while the angular velocity is taken to be the surface velocity of the shaft. There is no flux across the shaft, and the gradients of the other variables are zero. At the centerline of the tank, the radial and the angular velocity components are zero. Besides, all r-direction gradients are zero because of symmetry along the centerline of the tank. At the surface of the rotating impeller, no slip condition applies, and the velocity is assumed to be equal to the velocity of the surface of the rotating impeller. The gradients of velocity, k, ε and concentration were assumed to be zero at the surface of the impeller because of no flux across the solid. Both k and ε are assumed to be zero, since there is no fluctuation at the surface of the solid.

Experimental Apparatus and Measurements

The reactor had the standard tank configuration as shown in Figure 3 with a 3.0 in. dia. Rushton turbine impeller and a variable speed motor to give impeller speeds of 100 to 750 rpm. The reactor was constructed from clear plexi-glass using a 17.0 in. section of 12.0 in. dia. pipe with the bottom and four 1.0 in. baffles made from 1/4 in. sheet. The reactor was inside a square glass tank, and mounted on two sides of this tank was acrylic plastic sheets used for x-ray viewing to diffuse light from the flood lights. The tank was on an optical bench that had mounts to reproduce the positions of the tank, camera and lights. An injection tube (3/18 in dia.) was positioned at the top of the impeller 45 degrees from adjacent baffles as shown in Figure 3.

Several reactions and indicators were evaluated for color change, and the reaction of hydrochloric acid with sodium hydroxide was selected which is one of the fastest known chemical reactions. This reaction has a rate constant of $1.4A10^{11}$ mole/ liter- sec (Banford and Tipper 1969).

1.0 N solutions of HCl and NaOH were used with phenol phthalein indicator that gave a visual transition in color between red in base ($pH \succeq 10.0$) and colorless in acid ($pH \preceq 7.0$).

A number of procedures were tried to determine the best conditions to measure the color change reaction, e.g. from colorless to color and reverse. The following procedure was the best to visualize the turbulent plume from the impeller. First, the reactor was made acidic with an excess of 10 ml HCl. Then, 5 ml of NaOH was injected at the tip of the impeller. A colored plume developed and was transported around the reactor as the base was neutralized. The plume developed and disappeared in about 7.0 sec., and it was photographed with two video cameras using two 100-W flood lights as the only light source during the reaction.

Two charged-coupled-device, CCD, video cameras were used to capture two projections angles separated by a 90^o, as shown in Figure 6. The cameras were a COHU 6400 series and a Canon UCS2 8mm. Both cameras were set at the same focal distance of 48 inches and shutter speed of 1/1000 sec to get identical optical images of the stirred tank, and they capture optical images at a rate of 30 frames per sec.

Several stirrer speeds were investigated, and the best time for the reaction were obtained at a stirrer speed of 200 rpm. This speed gave a reaction time of 7.3 seconds while at 150 and 250 the reaction times were 4.1 and 10.5 seconds, respectively. At 200 rpm the Reynolds number ($D^2.N.\rho/\mu$) was 19,320, fully turbulent flow.

The HCl-NaOH reaction was analyzed from the beginning of the injection of NaOH until

the reaction completion after 7.3 seconds. During this time, a red plume develops and disperses as the reaction takes place. This gave a total of 219 (7.3x30) optical images which were digitized and used to reconstruct the three-dimensional concentration distributions in the reactor at intervals of 1/30 second. An optical image at 2.50 seconds of the reaction time is shown in Figure 7.

Image Processing and Analysis

The steps in image processing and tomography are shown in Figure 8. Optical images of the concentration fields captured by the video cameras during the reaction were displayed on a SONY Trinitron PVM-1343 MD color video monitor and recorded using a SONY EVO 9700 Hi8 video tape recorder (VTR). Individual frames of the recorded images were time-coded with the high resolution frame-by-frame advancing feature of the VTR. This features was required to obtain the exact order of the individual images when they were digitized using an AT&T TARGA-M8 imaging board which was installed in a Kenitec 486 DX2/66 MHz computer. This board was used with the Image-Pro® Plus 2.0 of Media Cybernetics image processing software to capture individual frames from the VTR and digitize the values of the intensity of the individual pixels into ASCII code. Then the intensities were converted to grey level intensities that range between 0 and 255, (0=black, 255=white), and each video camera digital image was stored in an individual file.

The files of the gray level intensities of the digitized optical images were used for the spatial reconstructions of the turbulent concentration fields in the stirred reactor. A Fortran computer program was written that uses the ART algorithm to compute the three-dimensional reconstruction of the concentration fields with the digital images from the two projections as described below. Each reconstruction calculated the concentration at points in the three-dimensional cylindrical grid having a height and diameter of 329 pixels or 27,969,040 grid points. These results were transferred to an IBM RS/6000 workstation and displayed using MATLAB.

The gray level intensity is a measure of hydroxyl ion concentration values. Pre-determined concentration value of the hydroxyl ion, C_{OH^-}, were video taped and processed to get the following relation of C_{OH^-} as a function of the gray level intensity;

$$\log_{10} C_{OH^-} = -0.000589 \cdot 0.031 \cdot GI - 3 \qquad (15)$$

This equation was used to evaluate the hydroxyl ion concentration from the measured gray level intensity.

The algebraic reconstruction technique (ART) is an iterative method where elements of the image matrix are computed from projection data (Hesselink, 1989). The image matrix is represented by the cross-hatched area in Figure 2 where the intersections are pixels. The concentration field is evaluated at these points throughout the reactor. The tank cross section was divided into a 329 by 329 grid as shown in Figure 9. The number of grid points was determined by the pixel resolution of the CCD video cameras and the view of the reactor.

The ART algorithm can be written for a horizontal plane k through the circular cross-section of the reactor by the equations given below for two projections. Two projection angles are used, and the equations for the ART algorithm are shown in Figure 10. Referring to Figure

10, $P_v(i,k)$, and $P_v(j,k)$ are the digital image data from the first and second projections, respectively. These are used to reconstruct the concentration field in the reactor, $f(i,j,k)$, at each point i,j,k. In these equations, q is the iteration counter, and a relaxation factor ε is that ranges between zero and unity is used to get optimum convergence.

The tomographic reconstruction of the concentration field starts at the top of the measurement volume. The following steps are used in reconstructing the concentration distribution for each horizontal cross section in the reactor. First, set all grid points to zero, $f(i,j,k)^o = 0$, and then projection values from digital images files, $P_v(i,k)$, and $P_v(j,k)$ are used with the equations for the x- and y- direction to determine new values of f(i,j,k) at the grid points. These equations are used iteratively until the convergence criterion is met for the current relaxation factor. The relaxation factor is increased from 0.1 to1.0 based on the value for the variance. Convergence is achieved when the variance is minimized, and the procedure continues to subsequent horizontal cross sections of the reactor until the concentration field of the entire measurement volume is reconstructed. Each reconstruction determined concentrations in a three-dimensional cylindrical grid with a diameter and height of 329 pixels or 27,969,040 grid points.

The accuracy of the tomographic reconstruction was evaluated three ways. These included measuring a stationary object, comparing the variance at points using the convergence criteria, and reconstruction of projections from the point concentrations. The variance from the convergence criteria gave a 1.7% error in the concentration measurements at a point. Also, the projections were determined from the point concentrations, and agreement was within 2.0%. A stationary object, a bottle with red liquid from phenol phthalein indicator, was reproduced within the accuracy of the dimensions of the bottle.

Reconstruction Results

The concentration variations at three points were evaluated at the locations shown in Figure 11 which would be what is obtained with a stationary probe. The results are shown in Figure 12, and this gives an indication of the typical rapid concentration fluctuations from the turbulent flow in the impeller region. The three points were located 4.5 mm from the impeller tip with point one at 31.0 mm above the centerline, point two at the centerline, and point three at 31.0 mm below the centerline. A relative concentration was used for convenience which is 100-gray level intensity to avoid the logarithmic nature of the hydroxyl ion concentration. The highest gray level intensity of 100 represents the lowest concentration. Dimensionless time is the actual measurement time divided by the total reaction time (7.3 sec.). The three curves shown in the figure connect points that are spaced at intervals of 1/30 second.

In Figure 13, the hydroxyl ion concentration is shown as a function of the radial distance from the impeller region at different planes from the liquid surface. The radial distance was made dimensionless by dividing the radial distance of the point of measurement by the distance between the impeller tip and the baffle edge. At 2.50 seconds into the reaction, the hydroxyl ion concentration was found to be inversely proportional to the dimensionless radial distance in the stirred tank. . This concentration dependence on radial distance from impeller area was reported by Manning, and Wilhelm, 1963 in their study of the concentration fluctuation in a stirred baffled vessel.

In Figure 14, some typical results for the angular dependence of the hydroxyl ion concentration as a function of time show the random fluctuations of the turbulent concentration

fields. The fluctuations increase as the plume of the reaction passes the points of measurements and then decline as the reaction goes to completion with the base, NaOH, being neutralized.

Validation of the the Flow Field with the RNG k-ε and Sliding Mesh Method

The three-dimensional solution of the RNG k-ε and sliding mesh method was validated with experimentally measured velocity profiles in the impeller stream region as shown in Figure 15. The impeller region flow is a tangential jet with a periodic steady state because of the passage of blades. The velocity simulation results in the stirred tank are close to the experimental data of different investigators as shown in Figure 15.

Evaluation of the Concentration Field with Chemical Reaction

The turbulent RNG k-ε model and the Ziman and Middleton closure model, Equations 11 and 12, with the aid of the moving-mesh technique was used with the kinetics of the HCl-NaOH neutralization reaction to predict the concentration field in the stirred reactor. The three-dimensional experimental data from optical tomography for the above reaction were used to establish the accuracy of the simulation. The optical tomography data was time-averaged using a time interval of one third of a second. This corresponds to the averaging of 10 concentration values, since each image is captured in one thirtieth of a second.

In Figure 16, the simulation NaOH concentration is shown as a function of dimensionless radial distance at different height of z'=0.16(z=0.24 inch) and z'=0.81 (z=1.22 inch) in the stirred tank at reaction time 2.5 second and compared with the time-averaged concentration. The dimensionless radial distance is obtained by dividing the radial distance by the distance between the impeller tip and the baffle edge. At 2.50 seconds into the reaction, the NaOH concentration was inversely proportional to the dimensionless radial distance at different heights in the stirred tank.

In Figures 17, 18 and 19 the NaOH concentration predicted by the simulation is shown as a function of time at the points given in Figure 11. Also shown are the measured concentrations (time-averaged) of NaOH. There is general agreement of the simulation with measurements through the time span. In these figures dimensionless time is real time divided by 7.3 seconds. Comparing the positions of the points shown in Figure 11, the one closer to the injection point has a maximum concentration is higher than the other two points. Less NaOH is transported to these two points.

Conclusions

A new method of measuring turbulent concentration fields in a stirred chemical reactor was developed using optical tomography and image processing. The system used the color change reaction of HCl and NaOH with phenol phthalein indicator to measure the concentration field at 27.9 million points at 1/30th sec. intervals in a stirred chemical reactor noninvasively using images from two perpendicular CCD video cameras. The reactor had a standard configuration (29.21 cm. dia., Rushton turbine).

The tomographic algorithm, algebraic reconstruction technique (ART), was used to reconstruct the three-dimensional concentration distribution from digitized video images

(329x329 pixels) of side views of the reactor. A plume of color was generated by injecting 5 ml of 1.0 N NaOH at the tip of the impeller an acidic solution in the reactor, and this plume moves around the reactor and collapses as the base is neutralized in 2.5 sec. at an impeller speed of 200 rpm. The concentration fields were reconstructed in 1/30th sec. intervals, and results are presented in several different forms, e.g. concentration at key points as a function of time. Validation included reconstruction of a stationary object, recalculation of projections and minimizing the error variance. The results of reconstructions showed the capability of tomography to represent the hydroxyl ion concentration in the stirred tank from two projection angles. A three-dimensional grid of $329 \times 329 \times 329$ data points in each reconstruction representing the gray level intensities in the measurement volume. The gray level was related to the hydroxyl ion concentration by a calibration experiment. Projection views were captured using two video cameras at a rate of 30 frame per second and reconstructions were made and utilized for the specified planner location in the stirred tank.

For the HCl-NaOH reaction at a stirred speed of 200 rpm, the hydroxyl ion concentration was found to be dependent on the radial distance from the impeller. Numerical values for the concentration fluctuations were presented at specified regions. These concentration fluctuation values can be further utilized to help solve the species continuity equations in the stirred tank.

For the simulation of turbulent flow, the RNG k-ε model proved to be one of the best models to simulate fluid flow. The velocity simulation results were close to the experiment data by previous researchers. The RNG k-ε model can be used with confidence to simulate the fluid flow in most situations.

Sliding mesh method was used to solve moving boundary problem and more detailed information around impeller was given. With the sliding mesh technique, jet model is not required in the simulation of turbulent fluid flow in a stirred reactor.

For the simulation of the turbulent chemical reaction in a stirred tank, the simulation concentration trend matches the concentration field for the chemical reaction experiments.

Nomenclature

c	Fluctuation concentration
$c_A c_B$	Covariance of fluctuation concentrations of species A and B
C_A	Concentration of species A
C_B	Concentration of species B
$\bar{C}_A$	Time-averaged concentration of species A
$\bar{C}_B$	Time-averaged concentration of species B
C_{OH^-}	Concentration of the hydroxyl ion
$\bar{C}_{OH^-}$	Time-averaged concentration of the hydroxyl ion
D	Shaft diameter
$f(i,j,k)$	Flow field variable (concentration)
GI	Gray level Intensity
i,j,k	Cartesian coordinates counters
k	Reaction rate constant, Equations 2 and 3.
N	Stirrer speed

N_i Number of grid points in the y-direction, Figure 4.
N_j Number of grid points in the x-direction, Figure 4.
N_{Re} Reynolds Number
$P_v(i,k)$ Projection element value in the y-direction
$P_v(j,k)$ Projection element value in the x-direction
q Iteration counter
r_A Reaction rate of species A

$\bar{r}_A$ Time-averaged reaction rate of species A
t time of measurement
t' Dimensionless time = t / total reaction time.
V_q Variance of the qth iteration

Greek Symbols
μ Viscosity
ρ Density

REFERENCES

Akiti, O. And P. M,. Armenante, 2004, "Experimentally-Validated Micromixing-Based CFD Model for Fed-Batch Stirred Tank Reactors," *AIChE Journal*, Vol. 50, No. 3, p. 566-577.

Armenante, M. P. and Chou, Chun-Chiao, 1996, "Velocity Profiles in a Baffled Vessek with Single or Double Pitched-Blade Turbines, AIChE Journal, Vol 42, No. 1, p. 1.

Bakker, A., and J. B. Fasano, 1994, "Pinpoint Mixing Problems with Laser and Simulation Software," *Chemical Engineering*, Vol. 101, No. 1, p. 94-100.

Banford and Tipper, 1969 complete

Bird, R.B., Stewart, W.E., and Lightfoot, E.N., 2002, *Transport Phenomena,* Second Edition, John Wiley and Sons, NY .

Bourne, J. R., F. Kozicki and P. Rys,1981, "Mixing and Fast Reactions I: Test Reactions to Determine Segregation," Chem. Eng. Sci., Vol. 36, p.1643.

Buchmann, M, and D. Mewes, 1998, "Measurement of the Local Intensity of Segregation with the Tomographical Dual Wavelength Photometry," *Canadian Journal of Chemical Engineering*, Vol. 76, p. 626-630 (June, 1998)

Chin Y. P., 1992, "A Moving Mesh Technique for Simulation of Flow in Mixing Tanks." AIChE Winter Annual Meeting on Numerical Simulation of Mixing Phenomena.

Corrsin, S., 1964, "Simple Theory of an Idealized Turbulent Mixer," AIChE Journal, Vol. 10, p.870.

Demirdzic, I. and M., Peric, 1990, "Space Conservation Low in Finite Volume Calculations of Fluid Flow," Int. J. Num. Methods in Fluids, Vol 8**,** p.1050(1990).

Eyring, G., and Eyring, E. M. 1963, Modern Chemical Kinetics Reinhold. New York, NY.

Fluent User's Guide Version 4.3, 1995, Fluent Inc. Lebanon, NH.

Fox, R. O., 2003, *Computational Models for Turbulent Reacting Flows*, Cambridge University Press,Cambridge, UK

Galletti, C., A. Paglianti, K. C. Lee and M. Yianneskis, 2004, "Reynolds Number and Impeller Diameter Effects on Instabilities in Stirred Vessels,' *AIChE Journal*, Vol. 50, No. 9, p. 2050-2063.

Haarde, W., Das *Vermischen mit Hilfe von Flussigkeitrahlen,* 1989, Ph. D. Dissertation, Universitat Hannover, Hanover, Germany.

Harvey D. A. and S. E. Rogers, 1996, " Steady and Unsteady Computation of Impeller-Stirred Reactors," AIChE Journal, Vol 42, No. 10, p. xx

Hesselink, L., "Optical Tomography," *Handbook of Flow Visualization*, 1989, W. J. Yang, Ed. Hemisphere Pub. Co., New York, NY, p. 321.
Herman, C. V., D. Mewes and F. Mayinger, 1992, "Optical Techniques in Transport Phenomena," *Advances in Transport Processes VIII*, Ch.1, p. 1-58, A. S. Mujumdar and R. A. Mashelkar, Eds., Elsevier Publ., New York.

Holden, P. J., M. Wang, R. Mann, F.J. Dickin and R. B. Edwards, 1998, " Imaging Stirred-Vessel Macromixing Using Electrical Resisance Tomography," AIChE Journal, Vol. 44, No. 4, p. 780-790.

Magnussen, B.F. and Hjertager, B. H., 1976, "On Mathematical Models of Turbulent Combustion with Special Emphasis on Soot Formation and Combustion m 16th Symp. (Int'l.) on Combustion, Cambridge, MA, Aug, p15-20, 1976.

Manning, F.S., and R. H. Wilhelm, 1963, " Concentration Fluctuation in a Stirred Baffled Vessel," *AIChE Journal* Vol. 9, p.12-19, .

Mao, K. W. and H. L. Toor, 1970, "Second-Order Chemical Reaction with Turbulent Mixing," *Ind. Eng. Chem. Fundam.*, Vol.11, p51.

Mavros, et al., 2001 complete

Middleton, J. C., 1985,"Computations of Flow Fields and Complex Reaction Yield in Turbulent Stirred Reactors and Comparisons with Experimental Data," *Chem. Eng. Res. Des*., Vol 64, p.

18.

Ostendorf, W. and D. Mewes,1988, “Measurement of Temperature Fields in Mixing Vessels using Optical Tomographt,” *Chem. Eng. Technol*, Vol 11p. 148.

Paul, E. L., V. A. Atiemo-Obeng and S. M. Kresta, 2004, *Handbook of Industrial Mixing: Science and Practice*, Wiley-Interscience, Hoboken, NJ.

Patterson, G. K., 1981, " Application of Turbulence Fundamentals to Reactor Modeling and Scale-up," *Chem. Eng. Commun.*, Vol.8, p25.

Perng, C. Y., and J. Y. Murthy, 1992, "A Moving-Mesh Technique for Simulation of Flow in Mixing Tanks," AIChE Ann. Meet., 1992.

Ranade, V. V., 1995, "Computational Fluid Dynamics for Reactor Engineering," *Reviews in Chemical Engineering,*Vol. 11, No. 3, p. 229.

Ranade, V. V. and J. R. Bourne, 1991, " Reactive Mixing in Agitated Tanks," *Chem. Eng. Commun*., Vol.99, p35,(1991).

Tatteson, G. B., 1991, "Fluid Mixing and Gas Dispersion in Agitated Tanks," McGraw, NY, p.278(1991).

Tatterson, G. B., 1990, *Fluid Mixing and Gas Dispersion in Agitated Tanks*, McGraw-Hill, New York.

Toor, H. L., 1969 " Turbulent Mixing of Two Species with and without Chemical Reactions," *Ind. Eng. Chem. Fundam.*, Vol.8, p. 580.

Toor, H., L., 1975, *Turbulence in Mixing Operations*, ed. Brodkey, R. S., Academic, NY, p.121.

Vassilatos, G. and H. L. Toor, 1965, "Second-Order Chemical Reactions in a Nonhomogeneous Turbulent Fluid," *AIChE J.*, Vol.11, p666.

Verschuren, I.. L. M., GJ. G. Wijers, J. F. Keurentjes, 2002, “Mean Concentration and Concentration Fluctuations in a Stirred-Tank Reactor,” AIChE Journal, Vol. 48, No. 7, p. 1390-1400.

Williams, R.A., Mann, R., Dickin F.J., Ilyas, M., and Ying, P., 1993, ”Application of Electrical Impedance Tomography to Mixing in Stirred Vessels," *AIChE Symposium Series*, Vol.293, p89.

Yalhot, V. and S. A. Orszg, 1986, “Renormalizion Group Analysis of Turbulence, I. Basic Theory," J. of Scientific Computing, Vol. 1, No. 1, p.1.

Ziman, H. J. and J. C. Middleton, 1990, " Computation of Mixing and Chemical Reaction in Stirred Vessels, " AIChE Annual Meeting, Chicago, Nov., 1990.

Figure 1 Schematic Representation of Tomography (Line Integrals)

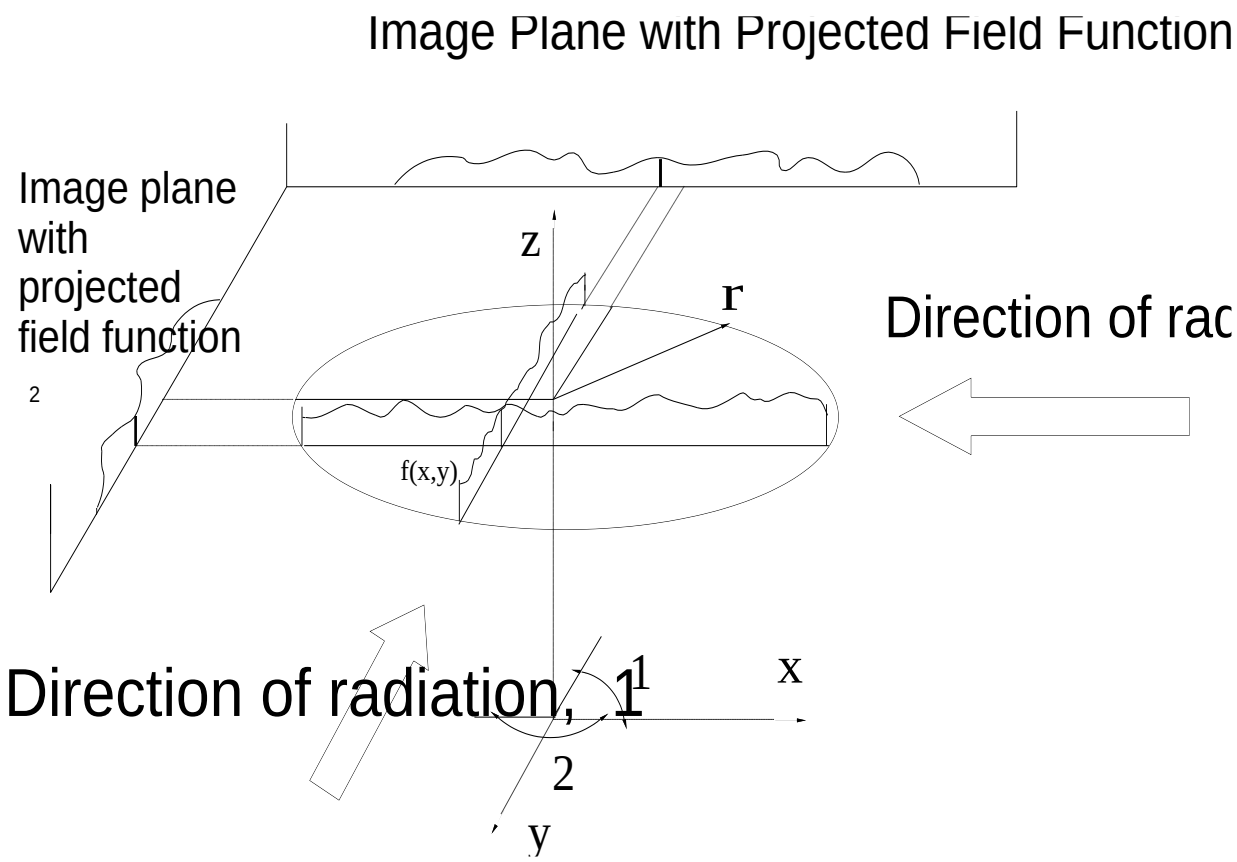

Figure 2 Cross Section in the

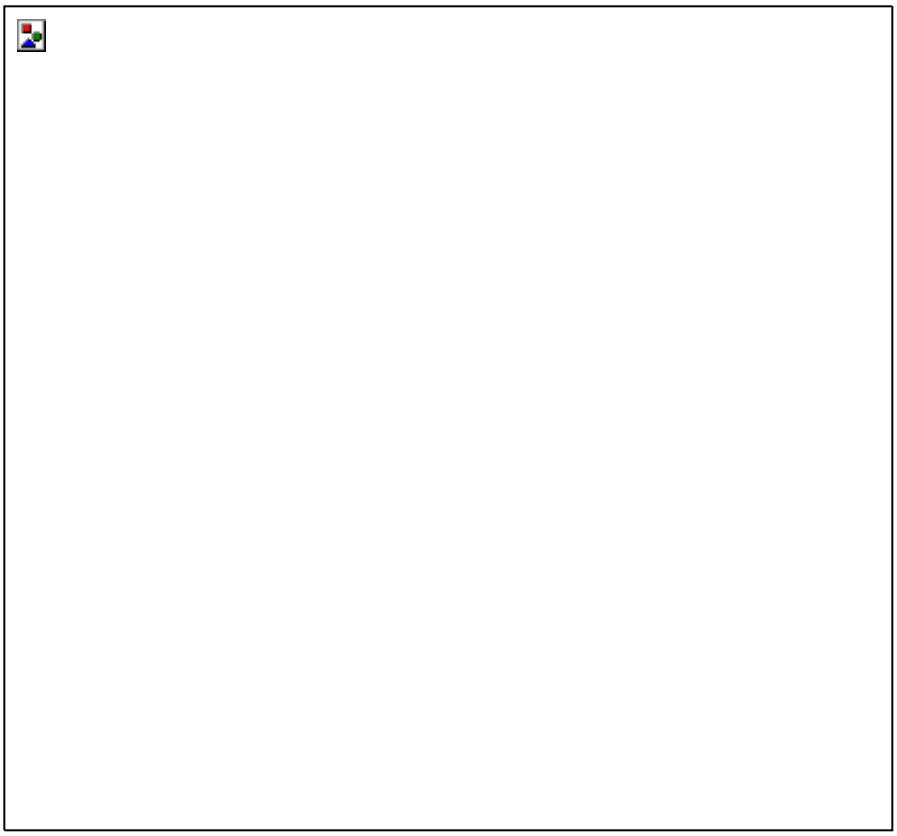

Measurement Volume Showing Pixel Locations at Grid Points

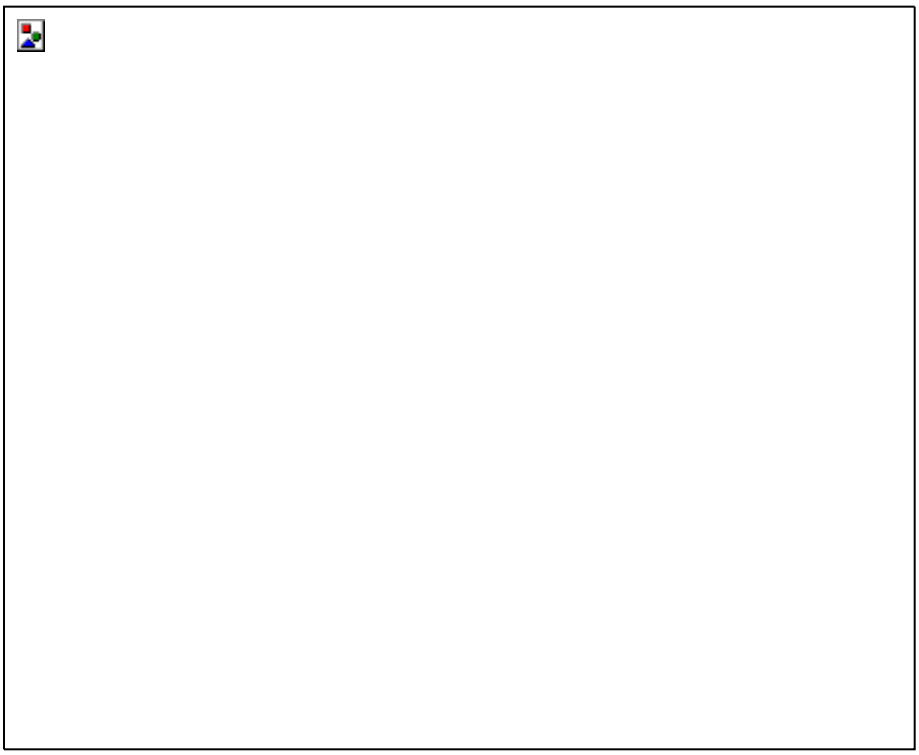

Figure 3 Standard Tank Configuration with a Rushton Turbine showing Location of Injection Tube

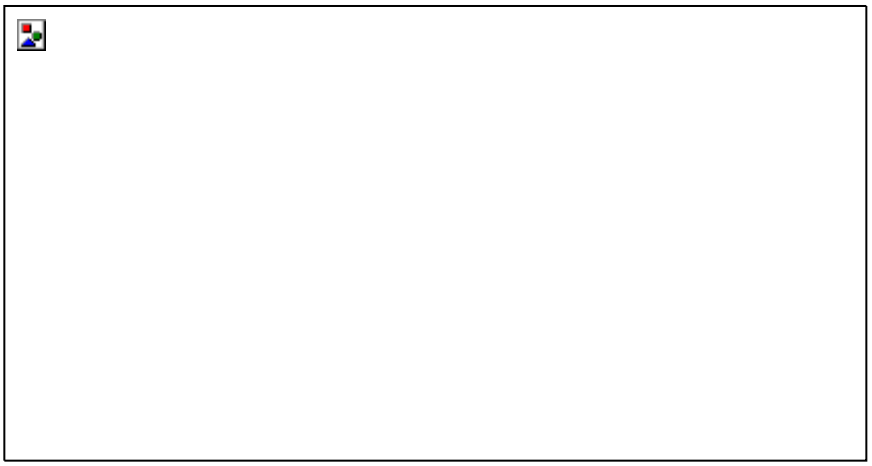

a. Initial Grid Distribution at Time t

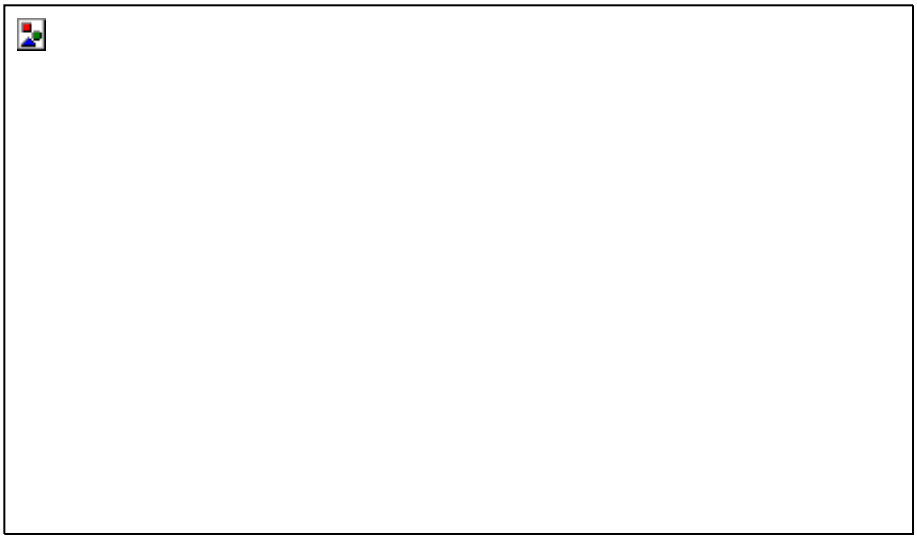

b. Grid Distribution after Time t+δt

Figure 4 Sliding Mesh Grid Distribution

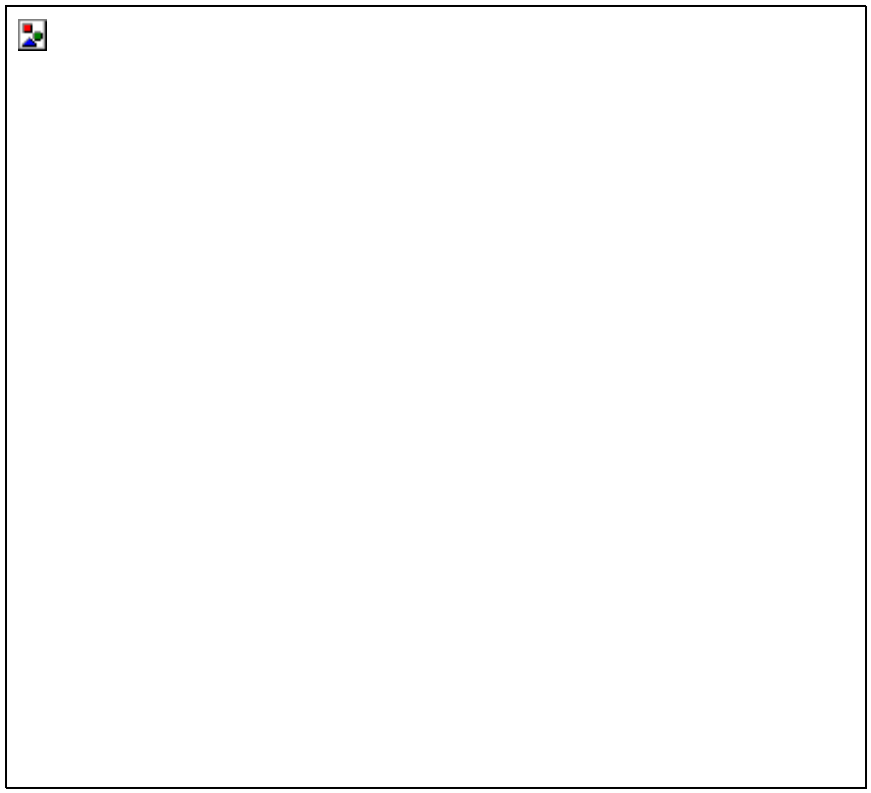

Figure 5 Boundary Conditions on the Stirred Reactor

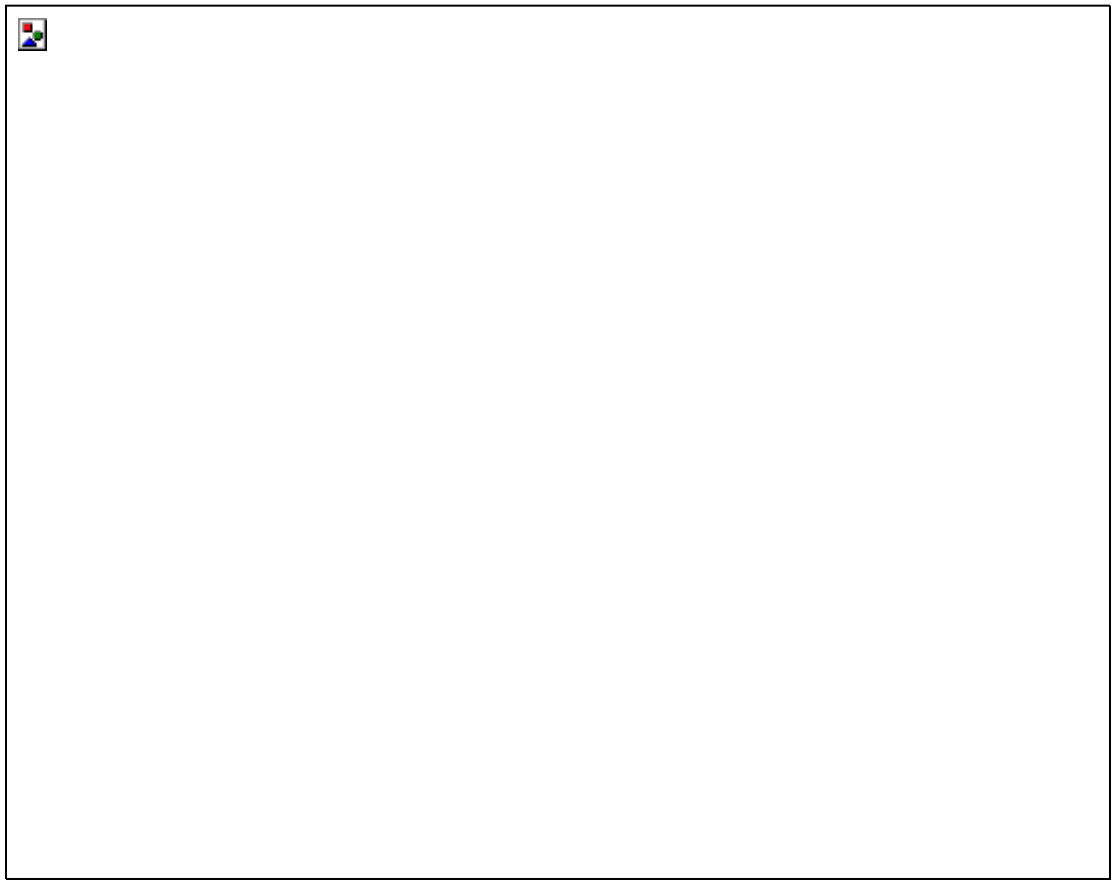

Figure 6 Video Cameras and Light Sources Relative to the Stirred Reactor

Figure 7 Gray Scale Intensities of the Optical Images Obtained from the Video Cameras for Stirrer Speed of 200 rpm and Reaction Time at 2.50 sec.

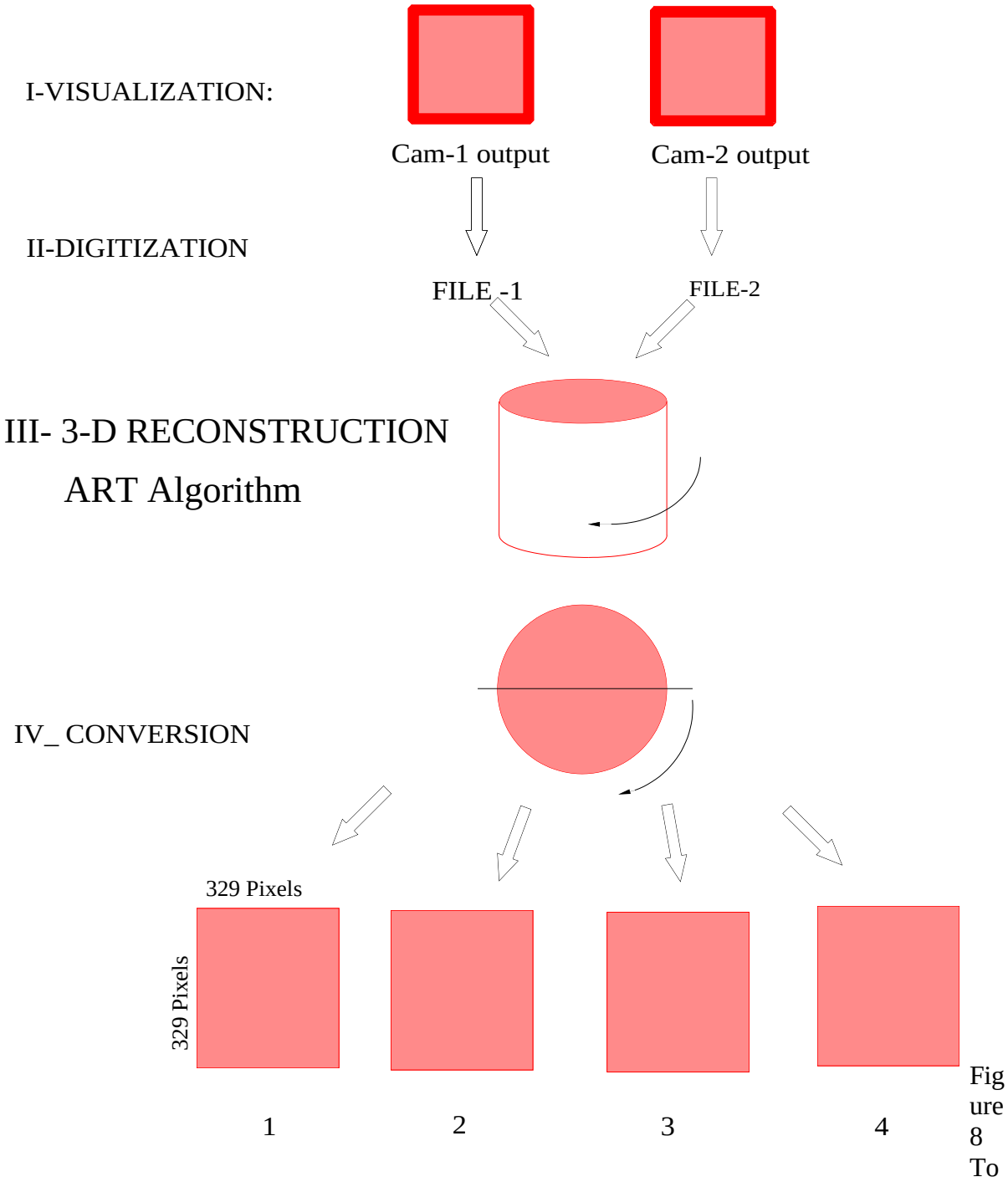

Figure 8 Tomography Reconstruction Methodology

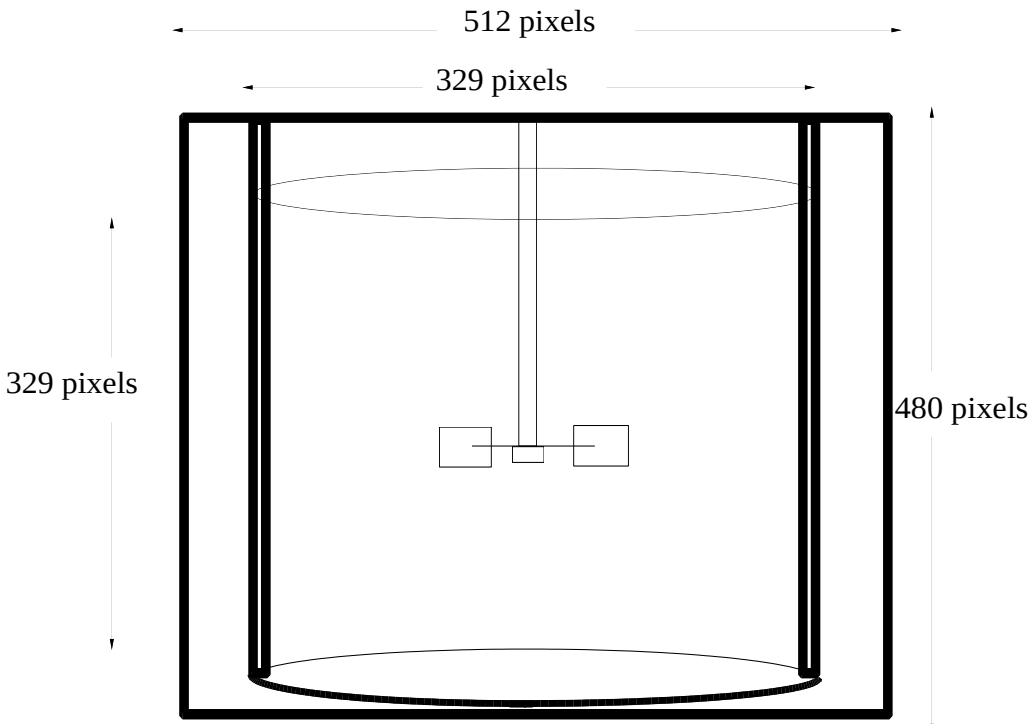

Figure 9 Camcorder Output and Pixel Determination

ART Algorithm:

X-direction

$$f_{ij}^{q+1} = f_{ij}^{q} + \frac{P_{vi} - \sum_{i=1}^{N} f_{ij}^{q}}{N_i}$$

Y-direction

$$f_{ij}^{q+2} = f_{ij}^{q+1} + \frac{P_{vj} - \sum_{j=1}^{N} f_{ij}^{q+1}}{N_j}$$

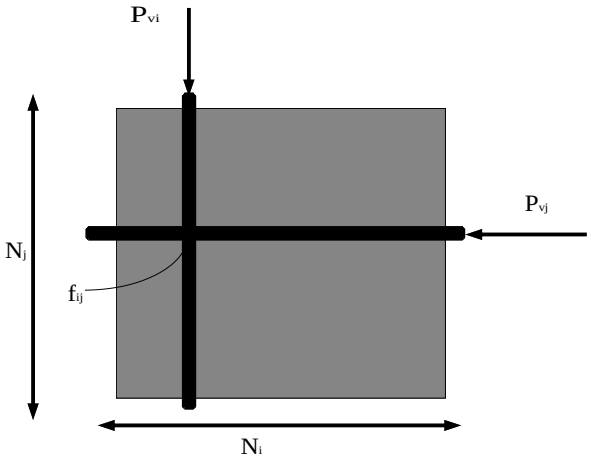

f_{ijq} = Grid point computed value (f_{ij0}=0).

P_{vi} = Line of sight projection value in the x -direction.

P_{vj} = Line of sight projection value in the y -direction.

N_i = No. of grid points in the x- direction.

N_j = No. of grid points in the y- direction.

Figure 10 Algebraic Reconstruction Algorithm (ART)

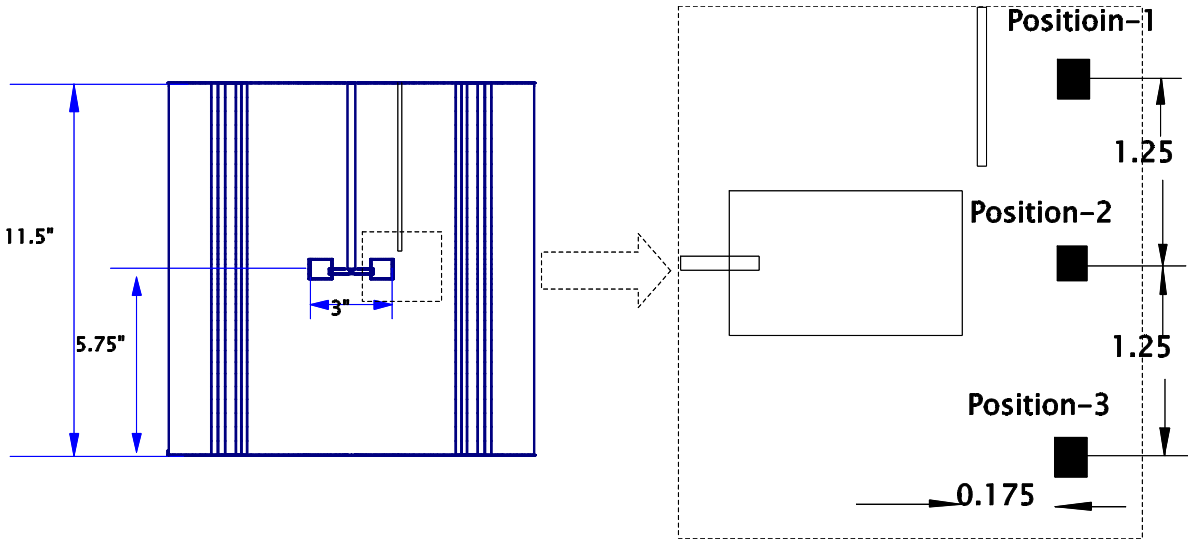

Figure 11 Location of Points Used to Simulate Measurements by a Fixed Probe

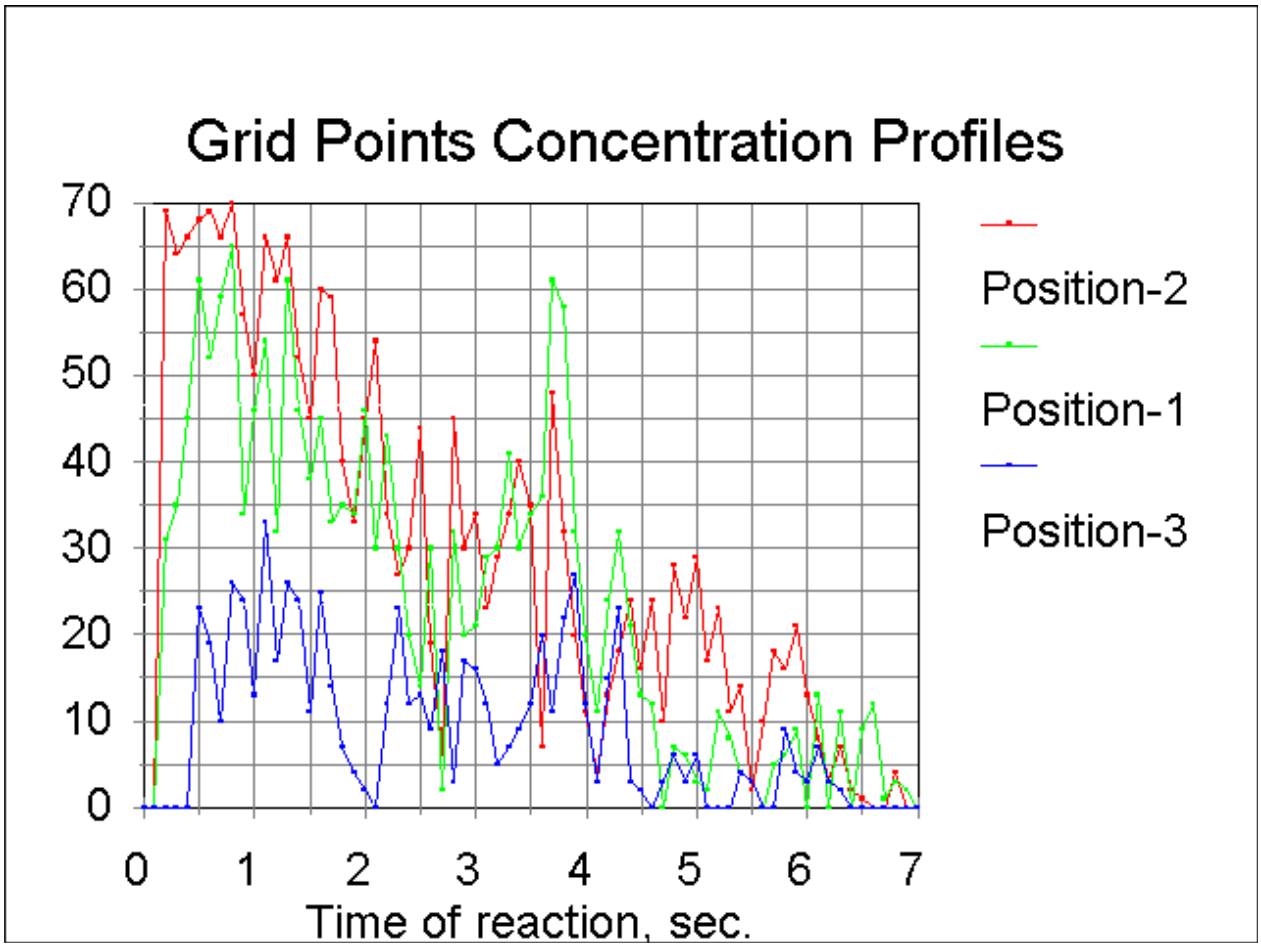

Figure 12 Relative Concentrations from Selected Points as a Function of Dimensionless Reaction Time. One-thirtieth of a Second Time Interval between Points

Figure 13. Hydroxyl Ion Concentrations a Function of Dimensionless Radial Distance at Six Heights from the Bottom, Stirrer Speed 200 rpm, Time 2.5 sec.

Figure 14 Hydroxyl Ion Concentration at Three Angles, 5.07 in from Top of Liquid, Stirrer Speed 200 rpm

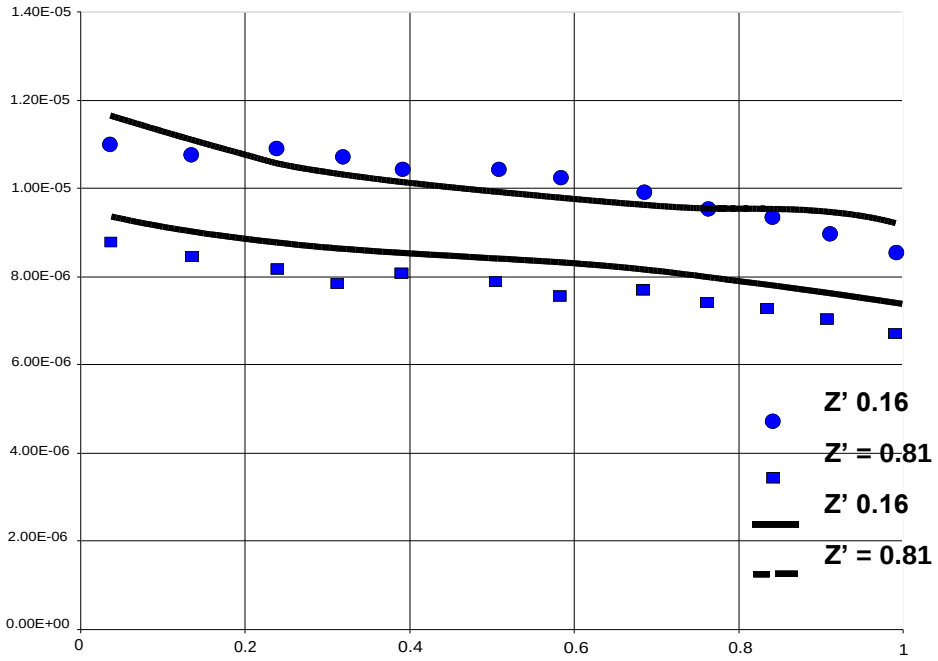

Figure 15 Comparison of NaOH Simulation and Experimental Concentrations as a Function of Dimensionless Distance

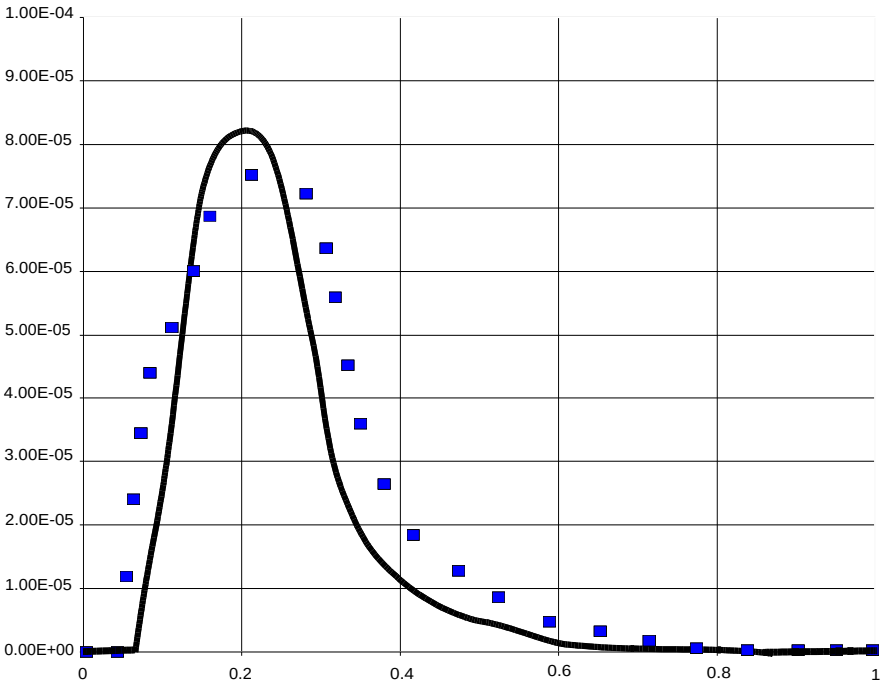

Figure 16 Local Point Comparison of NaOH Simulation and Experimental Concentrations as a Function of Time at Point 1 in Figure 12.

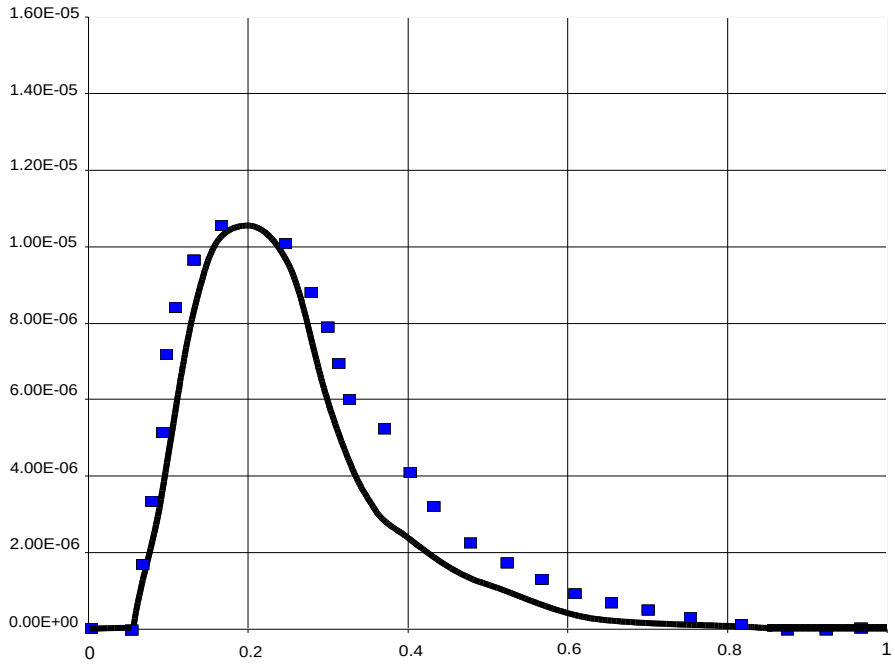

Figure 17 Local Point Comparison of NaOH Simulation and Experimental Concentrations as a Function of Time at Point 2 in Figure 12.

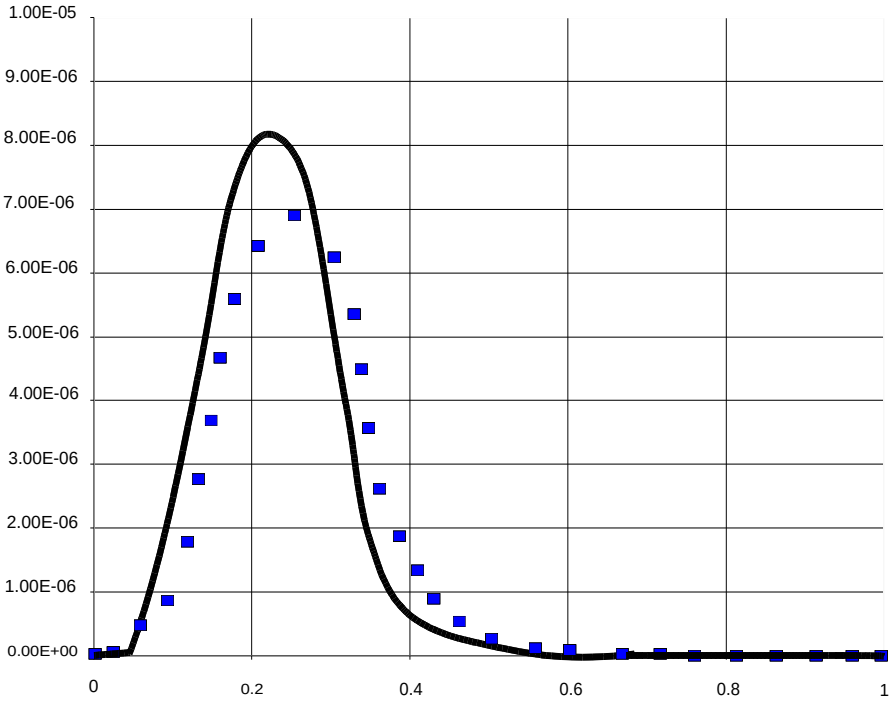

Figure 18 Local Point Comparison of NaOH Simulation and Experimental Concentrations as a Function of Time at Point 3 in Figure 12.

Figure 19 Comparison of Tangential and Radial Velocity Distributions in the Impeller Region with Experimental Data from Previous investigators